Mineralogical Magazine (2023), **87**, 599–610
doi:10.1180/mgm.2023.48

CAMBRIDGE UNIVERSITY PRESS

Article

The position of vanadium in the crystal structure of zoisite, variety tanzanite: Structural refinement, optical absorption spectroscopy and bond-valence calculations

Peter Bačík[1,2], Manfred Wildner[3], Jan Cempírek[4], Radek Škoda[4], Peter Cibula[1] and Tomáš Vaculovič[5]

[1]Comenius University in Bratislava, Faculty of Natural Sciences, Department of Mineralogy, Petrology and Economic Geology, Ilkovičova 6, 842 15 Bratislava, Slovak Republic; [2]Earth Science Institute of the Slovak Academy of Science, Dúbravská cesta 9, 84005 Bratislava, Slovakia; [3]Institut für Mineralogie und Kristallographie, Geozentrum, Universität Wien, Josef-Holaubek-Platz 2, 1090 Wien, Austria; [4]Masaryk University, Department of Geological Sciences, Kotlářská 2, 61137 Brno, Czech Republic; and [5]Department of Chemistry, Faculty of Science, Masaryk University, Kamenice 5, Brno 62500, Czech Republic

Abstract

Vanadium is the dominant trace element and chromophore in tanzanite, the most valued gemmological variety of zoisite. The structure of zoisite–tanzanite was obtained by structural refinement to assess the vanadium location in the zoisite structure. However, the small V content in tanzanite evidenced by electron microprobe and laser ablation inductively coupled plasma mass spectrometry limits the exact determination of the V position in the zoisite structure. Structural refinement revealed that the average bond length of the less distorted $M1,2O_6$ octahedron is below 1.90 Å, and $M3O_6$ has slightly longer bonds with an average of ca. 1.96 Å. The *M*1,2 site is slightly overbonded with a bond-valence sum (BVS) of 3.03 vu, whereas *M*3 is slightly underbonded (BVS = 2.78 vu). Optical absorption spectra revealed that most V is trivalent, but a small portion is probably in a four-valent state. Therefore, crystal field Superposition Model and Bond-Valence Model calculations were applied based on several necessary assumptions: (1) V occupies octahedral sites; and (2) it can occur in two oxidation states, V^{3+} or V^{4+}. Crystal field Superposition Model calculations from the optical spectra indicated that V^{3+} prefers occupying the *M*1,2 site; the preference of V^{4+} from the present data was impossible to determine. Bond-Valence Model calculations revealed no unambiguous preference for V^{3+}, although simple bond-length calculation suggests the preference of the *M*3 site. However, it is quite straightforward that the *M*1,2 site is better suitable for V^{4+}. If the possible octahedral distortion is considered, the $M1,2O_6$ octahedron is subject to a smaller change in distortion if occupied by V^{3+} than the $M3O_6$ octahedron. Consequently, considering the results of both the crystal field Superposition Model and Bond-Valence Model calculations, we assume that both V^{3+} and V^{4+} prefer the *M*1,2 site.

Keywords: zoisite, vanadium, octahedron, optical absorption spectroscopy, crystal field Superposition Model, bond-valence calculation

(Received 9 March 2023; accepted 14 June 2023; Accepted Manuscript published online: 29 June 2023; Associate Editor: Andrew G Christy)

Introduction

Zoisite, $Ca_2Al_3(SiO_4)(Si_2O_7)O(OH)$, is an orthorhombic sorosilicate crystallising in the *Pnma* space group (Liebscher *et al.*, 2002; Dörsam *et al.*, 2007). Zoisite is a polymorphic modification of clinozoisite and its structure (Fig. 1) is similar to that of the epidote supergroup but is formed by only one type of octahedral chain oriented in the *b*-axis direction (Fig. 2) (Liebscher *et al.*, 2002; Armbruster *et al.*, 2006). The structure of zoisite consists of seven cationic positions, of which two are surrounded by 7- to 9-fold coordination polyhedra (*A*1; *A*2), two by octahedra (*M*1,2; *M*3), three by tetrahedra (*T*1; *T*2; *T*3), and ten anionic positions, the O10 position being occupied by an OH group. Substitutions of Fe^{3+}, Cr^{3+}, Mn^{2+} and V^{3+} ions replacing Al^{3+} in the structure are commonly present (Dörsam *et al.*, 2007).

Zoisite was first described as 'saualpite', named after the Saualpe type locality in Carinthia, Austria. The name zoisite was given in 1805 by A. G. Werner, in honour of Siegmund Zois, Baron von Edelstein (1747–1819), an Austrian mineral collector, from whom Werner obtained the holotype of a new mineral from Saualpe (Gaines *et al.*, 1998). Zoisite occurs mainly in metamorphic and hydrothermally transformed rocks, and in pegmatites which were melted from eclogites (Franz and Smelik, 1995). Zoisite is a mineral that includes several colour varieties. The most sought-after variety of zoisite is tanzanite, whose blue-violet colour is caused by the presence of vanadium. Tanzanite was first identified by George Kruchiuk in 1962, who obtained several samples of alleged blue sapphire from the Merelani area of Tanzania (Dirlam *et al.*, 1992). At present, yellow, brown, green, blue–green and pink zoisites are mined on the site; these are often subjected to heat treatment to change the colour to exclusively blue (Zancanella, 2004).

The goal of this work is to determine the possible structural position of vanadium in the zoisite var. tanzanite structure. A fragment of blue tanzanite from the Merelani area, Tanzania (from the personal collection of Peter Bačík) was investigated

Corresponding author: Peter Bačík; Email: peter.bacik@uniba.sk
Cite this article: Bačík P., Wildner M., Cempírek J., Škoda R., Cibula P. and Vaculovič T. (2023) The position of vanadium in the crystal structure of zoisite, variety tanzanite: Structural refinement, optical absorption spectroscopy and bond-valence calculations. *Mineralogical Magazine* **87**, 599–610. https://doi.org/10.1180/mgm.2023.48

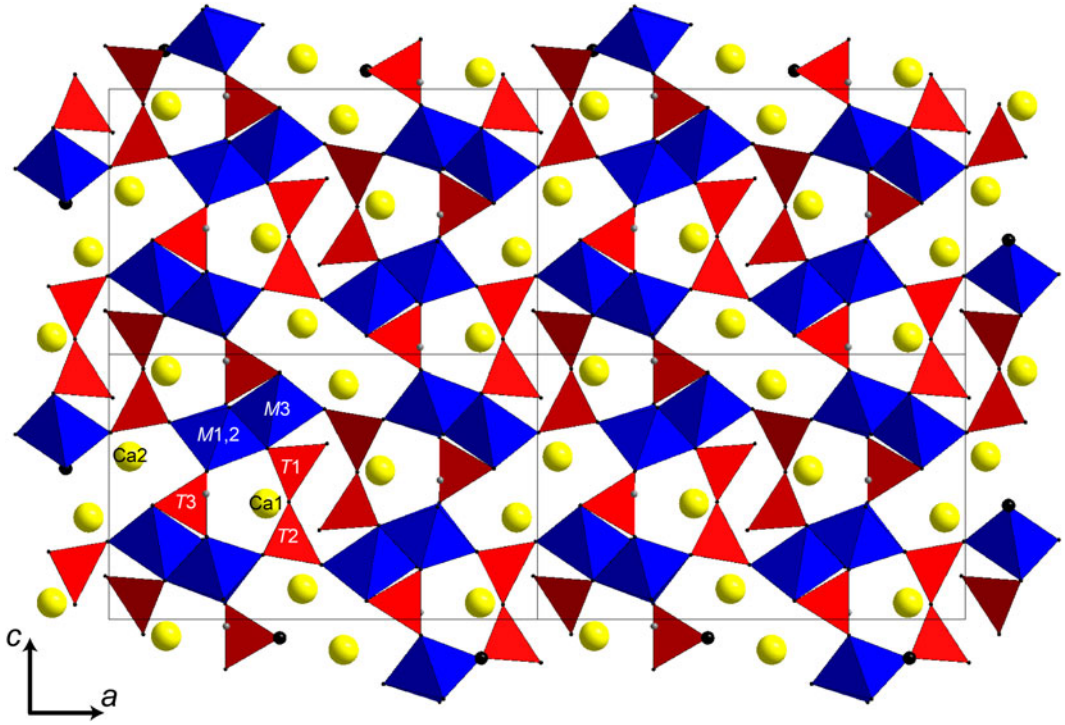

Fig. 1. Visualisation of the zoisite structure in a view perpendicular to *b* for the sample studied. Yellow = Ca; blue = octahedra, *M*; and red = tetrahedra, *T*. Drawn using Crystal Impact *Diamond* (version 3.2k).

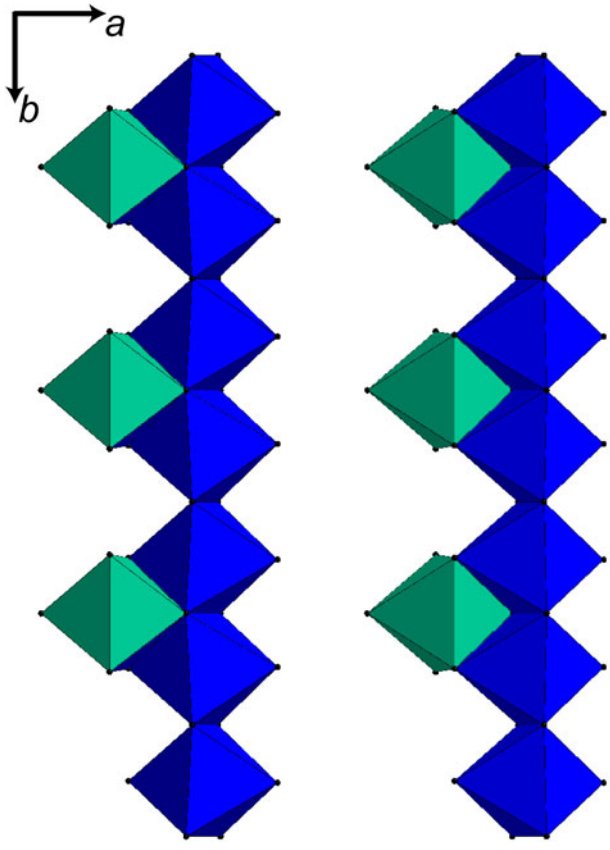

Fig. 2. The chains of $M1,2O_6$ (blue) octahedra parallel to *b* with attached $M3O_6$ (green) octahedra. Drawn using Crystal Impact *Diamond* (version 3.2k).

by a multi-analytical chemical, structural and spectroscopic approach. Direct determination using structural refinement has limited application due to the small amount of vanadium in tanzanite. Therefore, we applied optical absorption spectroscopy with its interpretation using crystal field Superposition Model calculations and structural refinement accompanied by Bond-Valence Model calculations and considered the possible influence of vanadium and other substituents on the zoisite structure.

Geological settings

The Merelani area is located in the western part of the Lelatema antiform ~65 km from the city of Arusha in Tanzania (Malisa, 1998, 2004) and consists of granulite complexes of the Pan-African Mozambican zone (Muhongo and Lenoir, 1994). Merelani is a world-famous area of minerals of gemmological quality, also called the 'Gemstone Belt of East Africa'. Here, it is possible to find garnets (tsavorite, spessartine and rhodolite), ruby, sapphire, tanzanite, kyanite, diopside and many other minerals (Malisa, 2004; Le Goff *et al.*, 2010; Feneyrol *et al.*, 2013; Harris *et al.*, 2014). Notably, in addition to blue–violet V-bearing tanzanite, the Merelani area is also the unique occurrence of light blue V-bearing axinite-(Mg) (Jobbins *et al.*, 1975; Andreozzi *et al.*, 2000). The site extends along the Lelatema fault system, which consists of Proterozoic metasediments, graphitic gneisses, dolomitic marbles and shales. The rocks went through a metamorphic peak from 7.7 to 9.1 kbar and 600–740°C at 640 Ma, while the Lelatema fracture system formed during deformation at 560 Ma (Appel *et al.*, 1998; Muhongo *et al.*, 1999; Hauzenberger *et al.*, 2004, 2007; Malisa, 2004; Le Goff *et al.*, 2010). After the Pan-African tectonothermal event, there was a hydrothermal dissolution of rocks rich in Ca, Mg, CO_2, and SO_3 and also enriched in V, U, Sr, Zn and heavy rare earth

https://doi.org/10.1180/mgm.2023.48 Published online by Cambridge University Press

elements. Subsequently, fluids with these elements got into local fractures and fissures, where they reacted with the bedrock layers. This reaction resulted in the formation of tanzanite and other zoisite varieties, green grossular (var. tsavorite), diopside, quartz, graphite and calcite (Bocchio *et al.*, 2012).

Sample description and possible treatment

The crystal studied was a heat-treated fragment of uniformly blue colour up to 1 cm in size with inclusions of flaky graphite crystals. It is important to consider that blue tanzanites are artificially treated from original yellow, brown, green, blue–green and pink zoisites mined at Merelani, Tanzania. The temperature range of this treatment is from 350 to 700°C (Zancanella, 2004). Dichroism (actually trichroism, but with similar blue and bluish-green directions) observed in the sample studied indicates that this crystal was artificially heat-treated. Natural high-quality blue–violet tanzanite samples are very rare, most of the bright blue tanzanite in the market has undergone heat treatment (Yang *et al.*, 2021).

Analytical methods

Chemical composition determination

The composition of zoisite studied was established using a Cameca SX100 electron microprobe analysis (EMPA) in wavelength-dispersion mode at the Masaryk University (Brno, Czech Republic), Department of Geological Sciences, under the following conditions: accelerating voltage = 15 kV, beam current = 20 nA and beam diameter = 3 μm. The samples were analysed using the following standards (all *Kα* lines): hematite (Fe); Mn_2SiO_4 (Mn); TiO (Ti); wollastonite (Ca); andalusite (Al); Mg_2SiO_4 (Mg); titanite (Si); chromite (Cr); gahnite (Zn); vanadinite (V); Ni_2SiO_4 (Ni) and Co (Co). The measured element detection limits ranged from 150 to 700 ppm. The tanzanite crystal-chemical formula (Table 1) was calculated on the basis of 8 cations per formula unit, the OH content was calculated assuming OH = 1 apfu.

Table 1. Electron probe microanalysis and ionic proportions of V-zoisite (tanzanite) from Merelani, Tanzania.*

	wt.%	D.L.	S.D.		apfu
SiO_2	**40.23**	0.04	0.03	Si^{4+}	3.015
TiO_2	0.01	0.07	0.06	*T*	3.015
Al_2O_3	**33.47**	0.02	0.23	Ti^{4+}	0.001
V_2O_3	**0.21**	0.19	0.16	Al^{3+}	2.958
Y_2O_3	0.02	0.08	0.07	V^{3+}	0.013
La_2O_3	0.02	0.09	0.08	Mn^{3+}	0.001
Ce_2O_3	0.07	0.15	0.13	Mg^{2+}	0.006
Pr_2O_3	0.13	0.24	0.21	*M*	2.979
Nd_2O_3	0.08	0.20	0.18	Ca^{2+}	1.988
Gd_2O_3	0.23	0.37	0.32	Y^{3+}	0.001
Mn_2O_3	0.02	0.07	0.06	La^{3+}	0.001
MgO	**0.05**	0.02	0.02	Ce^{3+}	0.002
SrO	0.07	0.10	0.09	Pr^{3+}	0.004
CaO	**24.74**	0.04	0.29	Nd^{3+}	0.002
F	0.09	0.10	0.09	Gd^{3+}	0.005
Cl	0.02	0.04	0.03	Sr^{2+}	0.003
H_2O**	2.00			*A*	2.006
Total	101.44			F^-	0.020
O=F	−0.04			Cl^-	0.003
O=Cl	−0.01			OH^-	1.000
Total	101.39				

*Only contents of oxides highlighted in bold were convincingly above their detection limits, however the presence of other elements is very likely according to LA-ICP-MS.
**Calculated assuming OH = 1 apfu.
D.L. detection limit; S.D. –standard deviation

Instrumentation for laser ablation inductively coupled plasma mass spectrometry (LA-ICP-MS) at the Department of Chemistry, Masaryk University, Brno, Czech Republic consists of the laser ablation system Analyte G2+ (CETAC Technologies) emitting laser radiation of λ = 213 nm, and the quadrupole ICP-MS spectrometer Agilent 7900 (Agilent Technologies, Japan). The sample was enclosed in two-volume ablation cell Helex2. The ablated material was carried out from the cell by He flows of 0.600 and 0.300 l/min. Argon was admixed (1.0 l/min) into the helium flow before ICP-MS. NIST 610 standard was used for the optimisation of ICP-MS parameters with respect to maximal S/N ratio, oxide formation <0.2% (ThO^+/Th), and U^+/Th^+ <1.1%. The laser ablation of the sample was done under these optimised parameters: laser beam spot of 100 μm diameter, repetition rate of 20 Hz and laser beam fluence of 6.0 J/cm^2. Each spot was drilled for 60 s, and the pause between the ablation of individual spots was 30 s. Glass reference material NIST610 and normalisation on Al content was used for the quantification purpose. Respective detection limits for each element are included in Table 2.

Crystal structure refinement

A platy fragment extracted from the tanzanite sample was studied using single-crystal X-ray diffraction. The measurement was done at the Centre for Higher Order Structure Elucidation (C-HORSE) at the University of British Columbia, Canada, using a Bruker X8 APEX II diffractometer with graphite-monochromated Mo*Kα* radiation. Crystal data and details of the structure refinement are listed in Table 3. The structure was solved using *SHELXT* (Sheldrick, 2015) and symmetry-transposed to the earlier published zoisite structure model (Alvaro *et al.*, 2012). The *CrysAlis* (Oxford Diffraction Ltd.) and *SHELXL* (Sheldrick, 2015) program packages were used for data reduction and structure refinement, respectively, using neutral scattering factors and anomalous dispersion corrections for cation atoms and ionised species for oxygen (O^{2-}; Azavant and Lichanot, 1993). Atoms at all cation sites (Ca at Ca1 and Ca2; Al at *M*1,2 and *M*3; and Si at Si1, Si2 and Si3) were set to vary freely (tested both individually and simultaneously) however their deviations from full occupancies were negligible; therefore, full occupancies of all sites were used for final refinement. The position of the H(10) hydrogen atom was located on the residual electron-density map. The structure was refined in space group *Pnma* and converged to a final *R*1 index of 1.24% for 2051 reflections with $F_o^2 > 2\sigma(F_o^2)$ and 126 refined parameters. The refined atomic coordinates and displacement parameters are listed in Table 4 and selected geometric parameters in Table 5. The crystallographic information file has been deposited with the Principal Editor of *Mineralogical Magazine* and is available as Supplementary material (see below).

Polarised optical absorption spectroscopy

Polarised optical absorption spectra of the tanzanite samples investigated were recorded on double-sided polished crystal slabs in the spectral range 36000–3400 cm^{-1}, i.e. covering the near ultraviolet (UV), the visible (Vis) and the near-infrared (NIR) ranges of the electromagnetic spectrum. Slabs were prepared in two different orientations, i.e. (010) and (001), both in two different thicknesses (the former slab at 9.03 mm, then thinned to 2.05 mm, the latter one at 6.05 and 2.20 mm), on

https://doi.org/10.1180/mgm.2023.48 Published online by Cambridge University Press

Table 2. The trace-elements contents (in ppm) of V-zoisite (tanzanite) from Merelani measured with LA-ICP-MS.

Point #	Na	Mg	K	Sc	Ti	V	Cr	Mn	Fe	Co	Cu	Zn	Ga	Ge	As	Sr	Y	Zr	Sn
1	200	413	23	47	227	2009	184	132	152	1	2	5	127	9	0.3	1513	66	18	0.4
2	48	292	18	38	343	1642	160	123	118	1	0	3	109	10	0.3	1235	95	24	0.6
3	29	288	8	35	327	1624	163	116	116	0	<	2	105	9	0.3	1220	87	23	0.7
4	30	389	11	42	246	2081	196	128	143	1	0	4	131	9	<	1466	79	16	0.7
5	28	260	8	36	270	1855	164	113	123	0	<	2	105	9	0.3	1323	78	17	0.6
6	136	280	50	39	308	1718	213	127	235	1	1	2	101	9	0.5	1360	99	28	0.9
7	28	318	9	38	327	2003	175	127	129	1	0	3	123	10	0.3	1402	90	18	0.6
8	37	306	10	38	305	1997	175	126	128	1	0	3	122	10	0.4	1424	87	17	0.6
9	29	281	8	38	325	1607	160	118	113	0	0	2	107	10	0.3	1233	91	23	0.7
10	31	318	9	41	334	2012	180	128	135	1	<	3	122	11	0.5	1433	97	25	0.8
D.L.	6	0.1	4	0.1	0.3	0.0	0.3	0.2	1.3	0.03	0.1	0.5	0.02	0.3	0.2	0.01	0.1	0.1	0.2

Point #	Ba	La	Ce	Pr	Nd	Sm	Eu	Gd	Tb	Dy	Ho	Er	Tm	Yb	Lu	Pb	Th	U
1	35	31	67	9	32	8	2	9	1	9	2	5	1	4	1	0.9	6	16
2	30	46	99	13	45	12	3	13	2	13	3	7	1	6	1	1.1	11	23
3	30	40	87	12	43	10	3	12	2	13	3	7	1	6	1	0.9	9	19
4	35	28	66	9	34	9	3	10	2	11	2	6	1	6	1	1.2	9	20
5	31	43	97	13	47	11	3	12	2	11	2	6	1	5	1	1.0	9	14
6	33	48	95	13	47	12	3	14	2	14	3	8	1	7	1	1.3	10	21
7	35	36	84	10	39	10	3	12	2	13	3	7	1	5	1	0.8	6	18
8	38	38	87	11	42	11	3	12	2	12	3	7	1	5	1	1.0	7	17
9	28	46	99	13	46	12	3	12	2	12	3	7	1	6	1	1.0	10	18
10	35	56	128	15	56	13	3	14	2	13	3	8	1	6	1	1.3	12	19
D.L.	0.01	0.1	0.1	0.1	0.01	0.01	0.1	0.1	0.1	0.01	0.1	0.1	0.1	0.1	0.1	0.01	0.05	0.05

D.L. – detection limit.

the one hand to allow polarised measurements with the electric light vector parallel to the three crystallographic axes, on the other hand allowing recording of strongly different intensities of various absorption features with reliable S/N ratios. As the relevant literature on the mutual assignment of pleochroic colours, optical axes, crystal morphology and crystallographic axes for untreated as well as for heat-treated tanzanites is highly inconsistent (see respective comments by Deer *et al.*, 1986), the slab orientations and cell-axes directions were checked by X-ray diffraction, referring to the generally consistent assignment of $a \approx 16$, $b \approx 5.5$ and $c \approx 10$ Å. The spectroscopic measurements were performed in the sample chamber of a Bruker Vertex 80 FTIR spectrometer, using a calcite Glan-prism polariser and appropriate combinations of light sources (Tungsten or Xenon lamp), beam splitters (CaF_2-NIR or CaF_2-ViS/UV), and detectors (InGaAs-, Si- or GaP-diodes) to cover the desired spectral range, at measuring spots of 1–2 mm in diameter (the specific measuring spots were selected under a stereomicroscope, avoiding inclusions and cracks in the two sample slabs as far as possible). Hence, each full spectrum is combined from three partial spectral regions (36000–20000 cm^{-1}: spectral resolution 40 cm^{-1}, averaged from 512 scans; 20000–11000 cm^{-1}: resolution 20 cm^{-1}, 128 scans; 11000–3400 cm^{-1}: resolution 10 cm^{-1}, 64 scans), if necessary merged from respective measurements at different slab thicknesses. The subspectra were aligned in absorbance for a perfect match and calculated to linear absorption coefficient α (cm^{-1}). Observed transition energies for the crystal field calculations were extracted from the spectra by visual inspection.

Table 3. Crystal and refinement data for V-zoisite (tanzanite) from Merelani.

Crystal data	
Space group	*Pnma*
a (Å)	16.1805(3)
b (Å)	5.5466(1)
c (Å)	10.0276(2)
V (Å^3)	899.94(3)
Z	4
Crystal size (μm)	50 × 120 × 150
Data collection	
Radiation, monochromator	Mo*Kα*, graphite
2θ (°)	4.8–70
Total / unique F_o	16415 / 2144
$F_o > 2\sigma F_o$	2051
R_{int}, $R\sigma$	0.0230, 0.0124
Refinement	
Refined parameters	126
Range of *h*	$-25 \le h \le 26$
Range of *k*	$-8 \le k \le 8$
Range of *l*	$-15 \le l \le 16$
R_1 for $F_o > 2\sigma F_o$	0.0124
R_1 for all unique F_o	0.0134
wR_2	0.034
GooF (=*S*)	1.19
$\Delta\rho_{max}$ (e^- Å^{-3})	0.39
$\Delta\rho_{min}$ (e^- Å^{-3})	–0.24

Crystal field Superposition Model calculations

Crystal field (CF) calculations were performed in the framework of the semiempirical Superposition Model (SPM) of crystal fields, originally developed by Newman (1971) to separate the geometrical and physical information contained in CF parameters, taking into account the exact geometry of the coordination polyhedra in the respective phases. The SPM is based on the assumption that the CF can be expressed as the sum of axially symmetric contributions of all *i* nearest-neighbour ligands of the transition metal cation. The CF parameters B_{kq} (in Wybourne notation) are then obtained from:

$$B_{kq} = \sum_i \bar{B}_k(R_0)\left(\frac{R_0}{R_i}\right)^{t_k} K_{kq}(\Theta_i, \Phi_i) \quad (1)$$

where $\bar{B}_k$ are the 'intrinsic' parameters (related to a reference metal–ligand distance R_0), t_k are the power-law exponent parameters, both

https://doi.org/10.1180/mgm.2023.48 Published online by Cambridge University Press

Table 4. Fractional atomic coordinates and isotropic or equivalent isotropic displacement parameters (Å^2) for V-zoisite (tanzanite) from Merelani.

	x	*y*	*z*	U_{iso}*/U_{eq}	U^{11}	U^{22}	U^{33}	U^{12}	U^{13}	U^{23}
Si1	0.41077(2)	¾	0.28254(3)	0.00427(5)	0.00371(10)	0.00496(10)	0.00415(10)	0.000	0.00024(8)	0.000
Si2	0.08144(2)	¼	0.10602(3)	0.00423(5)	0.00379(10)	0.00469(10)	0.00421(10)	0.000	−0.00011(8)	0.000
Si3	0.16028(2)	¼	0.43545(3)	0.00398(5)	0.00368(10)	0.00464(10)	0.00362(10)	0.000	−0.00005(8)	0.000
*M*1,2	0.24967(2)	0.99681(4)	0.18978(2)	0.00445(4)	0.00448(8)	0.00399(8)	0.00489(9)	−0.00009(6)	0.00026(6)	0.00001(6)
*M*3	0.10605(2)	¾	0.30023(3)	0.00522(6)	0.00279(11)	0.00668(12)	0.00620(12)	0.000	0.00017(9)	0.000
Ca1	0.36656(2)	¼	0.43734(2)	0.00803(4)	0.00765(8)	0.01049(8)	0.00594(8)	0.000	0.00089(6)	0.000
Ca2	0.45203(2)	¼	0.11490(2)	0.00982(4)	0.01133(8)	0.01153(9)	0.00661(8)	0.000	−0.00014(6)	0.000
O1	0.13036(3)	0.99848(9)	0.14620(5)	0.00656(9)	0.00537(18)	0.00515(19)	0.0092(2)	0.00080(15)	−0.00142(15)	−0.00006(16)
O2	0.10131(3)	0.01287(9)	0.43024(5)	0.00640(8)	0.00631(19)	0.0065(2)	0.0064(2)	−0.00192(15)	0.00061(15)	−0.00076(15)
O3	0.35898(3)	0.99057(9)	0.24422(5)	0.00635(8)	0.00452(18)	0.00495(19)	0.0096(2)	0.00041(14)	−0.00107(15)	−0.00024(16)
O4	0.21884(4)	¾	0.30069(7)	0.00453(11)	0.0043(2)	0.0048(3)	0.0045(3)	0.000	0.0002(2)	0.000
O5	0.22779(4)	¼	0.31198(7)	0.00462(11)	0.0049(3)	0.0047(3)	0.0043(3)	0.000	0.0012(2)	0.000
O6	0.27163(4)	¾	0.05978(7)	0.00497(11)	0.0054(3)	0.0052(3)	0.0043(3)	0.000	0.0014(2)	0.000
O7	0.99122(4)	¼	0.16337(8)	0.00827(12)	0.0049(3)	0.0106(3)	0.0094(3)	0.000	0.0017(2)	0.000
O8	0.99657(4)	¾	0.29415(8)	0.00890(13)	0.0046(3)	0.0121(3)	0.0099(3)	0.000	−0.0022(2)	0.000
O9	0.42026(6)	¾	0.44367(8)	0.01546(16)	0.0191(4)	0.0234(4)	0.0039(3)	0.000	−0.0003(3)	0.000
O10	0.26751(5)	¼	0.07490(7)	0.00725(12)	0.0123(3)	0.0051(3)	0.0043(3)	0.000	0.0020(2)	0.000
H10	0.2735(15)	¼	0.974(3)	0.048(7)*						

*Isotropic displacement parameter (Å^2).

for each rank *k* of the crystal field, R_i are the individual metal–ligand distances and $K_{kq}(\Theta_i,\Phi_i)$ are the coordination factors calculated from the angular polar coordinates of the ligands. For details and comprehensive reviews on the SPM refer to Newman (1971), Newman and Ng (1989, 2000), Rudowicz *et al.* (2019), and (with geoscientific focus) Andrut *et al.* (2004).

The actual CF calculations were done using the *HCFLDN2* module of the computer program package by Y.Y. Yeung (Rudowicz *et al.*, 1992; Chang *et al.*, 1994; Yang *et al.*, 2004), which includes imaginary CF terms and is thus applicable to arbitrary low symmetries of all $3d^N$ electron systems. A suite of supplementary programs (Wildner, unpublished) was used to manage the input and output of the *HCFLDN2* program, in particular (i) for the transformation of atomic to polyhedral polar coordinates; (ii) for the systematic variation of intrinsic and power-law SPM parameters, as well as of the Racah parameters B and C; (iii) for the SPM calculation itself, giving the actual values for the B_{kq} parameters of the CF; (iv) for the corresponding communication with a slightly modified version of the *HCFLDN2* program (Yeung, pers. comm.); and (v) for the interpretation and evaluation of the *HCFLDN2* output results in terms of a reliability index for the agreement of calculated and observed transition energies.

According to the low point symmetries 1 (*M*1,2) and *m* (*M*3) of the potentially V (or other transition metal) -bearing AlO_6 polyhedra in zoisite, symmetrically unrestricted SPM calculations were performed; however, to reduce the number of variables (accompanied by reduced CPU time) and to improve the transferability of intrinsic $\bar{B}_k$ parameters, the power-law exponent parameters t_k were fixed at their ideal electrostatic values of $t_4 = 5$ and $t_2 = 3$. The reference metal–ligand distance R_0 for V^{3+} was set to 2.01 Å, the sum of the ionic radii (Shannon, 1976) of octahedrally coordinated V^{3+}, 0.64 Å, plus 1.37 Å for O^{2-} in three-to fourfold coordination and equalling the overall mean bond length in $V^{3+}O_6$ polyhedra extracted by (Schindler *et al.*, 2000). Cubically averaged Dq_{cub} values were calculated from the B_{kq} parameters via the rotational invariant s_4 (Leavitt, 1982).

Table 5. Selected geometric parameters (Å) for V-zoisite (tanzanite) from Merelani.

Si1–O8	1.5869(8)	*M*3–O8	1.7726(8)
Si1–O3 ×2	1.6218(5)	*M*3–O4	1.8249(7)
Si1–O9	1.6231(8)	*M*3–O2 ×2	1.9573(5)
<Si1–O>	1.6134	*M*3–O1 ×2	2.1071(6)
		<*M*3–O>	1.9544
Si2–O7	1.5691(7)		
Si2–O9	1.6282(8)	Ca1–O7	2.2557(8)
Si2–O1 ×2	1.6538(5)	Ca1–O3 ×2	2.4157(5)
<Si2–O>	1.6262	Ca1–O1 ×2	2.5076(5)
		Ca1–O6	2.5510(7)
Si3–O2 ×2	1.6257(5)	Ca1–O5	2.5733(7)
Si3–O5	1.6511(7)	Ca1–O9 ×2	2.9069(3)
Si3–O6	1.6637(7)	<Ca1–O>	2.5600
<Si3–O>	1.6416		
		Ca2–O7	2.3121(8)
*M*1,2–O4	1.8330(5)	Ca2–O3 ×2	2.4533(5)
*M*1,2–O10	1.8392(5)	Ca2–O2 ×2	2.5099(5)
*M*1,2–O3	1.8514(5)	Ca2–O2 ×2	2.7873(6)
*M*1,2–O5	1.8971(5)	Ca2–O8 ×2	3.0070(3)
*M*1,2–O6	1.9235(5)	Ca2–O10	3.0124(8)
*M*1,2–O1	1.9795(5)	<Ca2–O>	2.6840
<*M*1,2–O>	1.8873		

Bond-Valence Model calculations

Bond-length and bond-valence calculations are based on the following equations:

$$d_{ij} = R_0 - b\ln v_{ij} \quad (2)$$

$$v_{ij} = exp(R_0 - d_{ij}/b) \quad (3)$$

where d_{ij} is the bond length (in Å) between the two given ions, the bond valence (v_{ij}) measures the bond strength (in vu – valence units), R_0 is the length of a single bond (for which $v_{ij} = 1$ vu), and b is the universal parameter for each bond (Brown, 2006). The R_0 and b values for each cation from the list of Gagné and Hawthorne (2015) were used, as this list provides the most current and consistent data on the bonding parameters. For more details, see Bačík and Fridrichová (2019). Bond lengths were calculated only for the most common major, minor and trace elements occurring in zoisite, although a similar approach can be used for any chemical element.

https://doi.org/10.1180/mgm.2023.48 Published online by Cambridge University Press

Results

Chemical composition

The composition of the Merelani tanzanite based on the EMPA is close to pure zoisite (Table 1). Among the octahedrally coordinated cations, the most abundant is Al with limited substitutions of V and Mg. The amounts of other cations were below their detection limits. At the *A* sites, the observed amounts of Ca below 2 atoms per formula unit (apfu) allow for some substitution of Sr and rare earth elements, however, their contents are very near their respective detection limits. Tetrahedrally-coordinated sites are only occupied by Si.

The LA-ICP-MS analyses of the sample studied show that V and Sr are the most abundant among trace elements exceeding 1000 ppm. The contents of Mg, Ti, Cr, Mn, Fe and Ga vary between 100–450 ppm; those of Na, K, Sc, Y, Zr, Ba, La, Ce, Pr, Nd, Sm, Gd, Dy, Th and U are usually below 100 ppm; and the remaining elements are only slightly above their respective detection limits (Table 2). Moreover, the measurements from 10 points in the line profile show no significant variations in any of the measured elements and therefore, no significant zoning of the crystal studied.

Crystal structure refinement

The structure of V-zoisite from Merelani agrees with the previously reported data (e.g. Alvaro *et al.*, 2012). The zoisite structure is characterised by chains of edge-sharing *M*1,2 octahedra parallel to [010], decorated by *M*3 octahedrally coordinated sites that share edges with two *M*1,2 octahedra. Typically, the *M*1,2 octahedra are occupied by Al^{3+} whereas *M*3 can be occupied by both Al^{3+} and Fe^{3+} (Tsang and Ghose, 1971b; Alvaro *et al.*, 2012). The octahedral chains are linked by isolated SiO_4 tetrahedra (*T*3) in the *c* direction and by Si_2O_7 groups (*T*1 and *T*2) in the *a* and *c* directions; cavities in this framework of octahedra and tetrahedra contain two sevenfold- to ninefold-coordinated sites (*A*1 and *A*2) occupied by Ca. Hydrogen is bonded to oxygen O10 bonded to two *M*1,2 cations (Franz and Liebscher, 2004). The bond-valence analysis of the refined structure shows discrepancies between calculated bond valences and formal cation charges (Table 6) at all sites but *T*2 and *A*1.

The average bond length of the $M1,2O_6$ octahedron is below 1.90 Å; $M3O_6$ has slightly longer bonds with an average of ca. 1.96 Å (Table 7). The $M1,2O_6$ octahedron also has a smaller bond-length distortion than $M3O_6$. Its distortion parameter DI (Al–O) is 0.024, whereas that of $M3O_6$ is more than twice higher (Table 7). The difference in Δ_{oct} is even higher, in $M1,2O_6$ it is 0.77 and in $M3O_6$ it is as much as 4.21. Similarly, the $M3O_6$ octahedron is stronger bond-angle distorted than $M1,2O_6$; both DI (O–*M*–O) and σ^2_{oct} parameters of $M3O_6$ are higher: 0.057 *vs.* 0.040 and 47.33 *vs.* 20.67 (Table 8), respectively.

Optical absorption spectra

The polarised optical absorption spectra of the investigated tanzanite sample are shown in Fig. 3. Four major regions of absorptions can be distinguished: (1) the NIR region ≤ 6500 cm^{-1}, containing combination and overtone modes of fundamental vibrations that are not the focus of the present study (and not included in Fig. 3); (2) the NIR and Vis region between ~12000–23000 cm^{-1}, containing various CF absorption bands with maxima around ~13500 and 16500–19000 cm^{-1}, also including faint remains of the band at ~22000 cm^{-1} (in polarisation ∥ the *a*-axis) that is responsible for the colour-change of tanzanites upon heat-treatment; (3) an absorption band system centred around ~26500 cm^{-1}, i.e. close to the Vis-Near-UV boundary and thus still influencing the colour and pleochroism of tanzanites; and (4) the UV absorption edge, strongly ascending between 33000–34000 cm^{-1}, perhaps showing a faint structure in polarisation ∥ the *c* axis at ~34000 cm^{-1}. The bands or band components have half-widths typical for spin-allowed *d*–*d* CF-transitions, whereas there are no spectral features that could be attributed to respective field-independent (i.e. sharp) spin-forbidden transitions. The trichroism of the investigated tanzanite referring to the crystallographic axes, i.e. purple ∥ *a*, blue ∥ *b*, and bluish green ∥ *c*, can be correlated easily with the respective absorption behaviour within the visible spectral range between ~14000 and 25000 cm^{-1}.

Table 6. Bond valences (vu) for V-zoisite (tanzanite) from Merelani (BVS – bond-valence sum)

Si1–O8	1.10	*M*3–O8	0.70	BVS (O1)	1.87
Si1–O3 ×2	1.01	*M*3–O4	0.62	BVS (O2)	1.78
Si1–O9	1.00	*M*3–O2 ×2	0.44	BVS (O3)	2.13
BVS (Si1)	4.11	*M*3–O1 ×2	0.30	BVS (O4*)	1.82
		BVS (*M*3)	2.79	BVS (O5)	2.15
Si2–O7	1.15			BVS (O6)	2.06
Si2–O9	0.99	Ca1–O7	0.43	BVS (O7)	1.95
Si2–O1 ×2	0.93	Ca1–O3 ×2	0.29	BVS (O8)	1.94
BVS (Si2)	3.99	Ca1–O1 ×2	0.23	BVS (O9)	2.08
				BVS (O10*)	1.25
Si3–O2 ×2	1.00	Ca1–O6	0.21		
Si3–O5	0.93	Ca1–O5	0.20		
Si3–O6	0.90	Ca1–O9 ×2	0.09		
BVS (Si3)	3.83	BVS (Ca1)	2.04		
*M*1,2–O4	0.60	Ca2–O7	0.37		
*M*1,2–O10	0.59	Ca2–O3 ×2	0.26		
*M*1,2–O3	0.57	Ca2–O2 ×2	0.23		
*M*1,2–O5	0.51	Ca2–O2 ×2	0.12		
*M*1,2–O6	0.48	Ca2–O8 ×2	0.07		
*M*1,2–O1	0.41	Ca2–O10	0.07		
BVS (*M*1,2)	3.16	BVS (Ca2)	1.80		

*Hydrogen bond donor (O10) and acceptor (O4)

Bond-valence and bond-length calculation

Ideal bond lengths for typical octahedral cations in zoisite were calculated from the ideal bond valences of 0.5 vu for trivalent and 0.33 vu for divalent cations (Table 9). The Al–O bond has the shortest ideal bond length; other trivalent cations form slightly longer bonds, the largest difference (0.11 Å) was observed for the Fe^{3+}–O bond. For comparison, the difference in ideal bond lengths of divalent cations compared to the Al–O bond is >0.25 Å. Interestingly, the V^{4+}–O bond length is <0.02 Å larger than the Al–O bond.

This also makes V^{4+}–O the only bond (except Al–O) which is shorter than the average bond length of the $M3O_6$ octahedron – the larger of the two octahedra in the zoisite structure (Fig. 4). Bonds of trivalent cations (except Al) are longer than <*M*3–O> though the difference is not larger than 0.05 Å, which is less than ca. 2.5% of the bond length. The difference of Fe^{2+}–O and Mn^{2+}–O bond lengths to <*M*3–O> is 0.20 and 0.25 Å, respectively. This is equal to 10–13% of the <*M*3–O> bond length. The difference to <*M*1,2–O> is even larger, more than 16% in case of the Mn^{2+}–O bond.

As some works (Ghose and Tsang, 1971; Tsang and Ghose, 1971a) suggest the presence of V^{2+} as a possible chromophore

https://doi.org/10.1180/mgm.2023.48 Published online by Cambridge University Press

Table 7. Empirical bond lengths (in Å) at the octahedral sites of the sample studied compared to published data and calculated octahedral bond-length distortions.

Cation site	Anion	This work	Alvaro *et al.* (2012)	Liebscher *et al.* (2002)	Cation site	Anion	This work	Alvaro *et al.* (2012)	Liebscher *et al.* (2002)
*M*1,2	O4	1.8328	1.8412	1.8271	*M*3	O8	1.7723	1.7681	1.7364
	O-H10	1.8385	1.8432	1.8478		O4	1.8257	1.8313	1.8701
	O3	1.8515	1.8615	1.8647		O2	1.9574	1.9591	1.9341
	O5	1.8974	1.9014	1.893		O2	1.9574	1.9591	1.9341
	O6	1.923	1.9246	1.9311		O1	2.1075	2.1151	2.1286
	O1	1.9792	1.976	1.9917		O1	2.1075	2.1151	2.1286
Average		1.8871	1.8913	1.8926			1.9546	1.9580	1.9553
DI(*M*–O)		0.024	0.023	0.024			0.053	0.054	0.060
$\Delta_{oct} \times 10^3$		0.77	0.66	0.86			4.21	4.41	5.05

Distortion parameters: Bond-length distortion DI $(M-O) = \left(\sum_{i=1}^{6} |d_i - d_m|\right)/(6 \times d_m)$

Quadratic elongation $\Delta_{oct} = \frac{1}{6}\sum_{i=1}^{6} [(d_i - d_m)/d_m]^2$

in tanzanite, its ideal bond lengths were calculated in the octahedral, 7- and 9-fold coordination (Table 9). The calculation revealed that V^{2+}–O bonds in the octahedral coordination are significantly longer than average bond length of both octahedra in zoisite. In contrast, if we assume higher coordination, V^{2+}–O bonds are shorter than Ca–O bonds at both possible sites in zoisite with an even larger difference. Consequently, it is possible to conclude that the presence of any V^{2+} in tanzanite is highly unlikely.

Discussion

Estimation of the V position in the tanzanite structure in such low concentrations is based on several necessary assumptions. Firstly, it is well established that in zoisite, V occupies octahedrally-coordinated sites with an assumed preference of the *M*3 site (Ghose and Tsang, 1971; Tsang and Ghose, 1971a, 1971b). Then, the oxidation state of V is not straightforward. In the sample studied, the presence of any yellow–green shade typical for untreated tanzanite (Yang *et al.*, 2021) was not found and has probably been shifted to bluish green, hence we assume the heat treatment of the sample. This change in pleochroism was proposed to be the result of V^{3+} to V^{4+} oxidation or Ti^{3+} to Ti^{4+} oxidation (Schmetzer and Bank, 1978; Pluthametwisute *et al.*, 2020). This would indicate that a significant part of the V should be four-valent, while some V could remain in a trivalent state. Consequently, the position and oxidation state of V in the tanzanite structure was studied and derived from the optical spectra accompanied by CF calculations and the structure by the bond-valence calculations.

Crystal field Superposition Model calculations

The chemical analysis (Table 1) shows that V (1854 ppm) is by far the major transition element and hence will be decisive for the crystal field absorption spectra, with possible minor influence of Ti (301 ppm). Theoretically, vanadium as a V^{2+} or V^{3+} cation (with d^3 and d^2 *d*-orbital configuration, respectively), i.e. cations with a spectroscopic F ground term plus one spin-allowed excited P-term, could be responsible for the observed complex spectral envelope, though V^{2+} is neither compatible with available structural sites in zoisite, nor expected to be stable enough in oxidic environments (Faye and Nickel, 1971) or upon heat-treatment. Hence V^{3+}, substituting for aluminium in one or both available Al-sites, very probably dominates the absorption spectra. However, in the present case, V^{4+} and Ti^{3+}, both with d^1 configuration may also contribute to some extent.

Previous detailed crystal-field analyses of V^{3+} in tanzanite (Faye and Nickel, 1971; Tsang and Ghose, 1971a) assumed that

Table 8. Empirical bond angles (°) at the octahedral sites of the sample studied compared to published data and calculated octahedral bond-angle distortions.

Cation site	Anion 1	Anion 2	This work	Alvaro *et al.* (2012)	Liebscher *et al.* (2002)	Cation site	Anion 1	Anion 2	This work	Alvaro *et al.* (2012)	Liebscher *et al.* (2002)
*M*1,2	O4	O3	93.849	93.48	93.203	*M*3	O8	O2	89.069	89.291	89.181
	O4	O5	96.325	96.025	96.582		O8	O2	89.069	89.291	89.181
	O4	O6	85.983	86.07	85.89		O8	O1	99.285	99.207	99.579
	O4	O1	82.647	82.934	84.03		O8	O1	99.285	99.207	99.579
	O–H10	O3	92.81	92.779	92.517		O4	O2	92.285	91.973	91.81
	O–H10	O5	82.451	82.746	82.749		O4	O2	92.285	91.973	91.81
	O–H10	O6	95.161	95.112	94.659		O4	O1	79.349	79.377	79.285
	O–H10	O1	90.643	90.744	90.237		O4	O1	79.349	79.377	79.285
	O3	O5	90.095	89.683	91.038		O2	O2	96.299	96.495	97.073
	O3	O6	90.576	90.728	90.131		O2	O1	90.476	90.227	91.015
	O5	O1	87.543	87.398	87.765		O2	O1	90.476	90.227	91.015
	O6	O1	91.941	92.335	91.196		O1	O1	81.701	81.961	79.771
Average			90.002	90.003	90.000	Average			89.911	89.884	89.882
DI(O–*M*–O)			0.040	0.039	0.036	DI(O–Al–O)			0.057	0.056	0.061
σ^2_{oct}			20.65	19.42	17.66	σ^2_{oct}			47.32	46.45	52.52

Distortion parameters: Bond-angle distortion DI $(O-M-O) = \left(\sum_{i=1}^{12} |\alpha_i - \alpha_m|\right)/(12 \times \alpha_m)$

Octahedral angle variance $\sigma^2_{oct} = \frac{1}{11}\sum_{i=1}^{12} (\alpha_i - 90)^2$

https://doi.org/10.1180/mgm.2023.48 Published online by Cambridge University Press

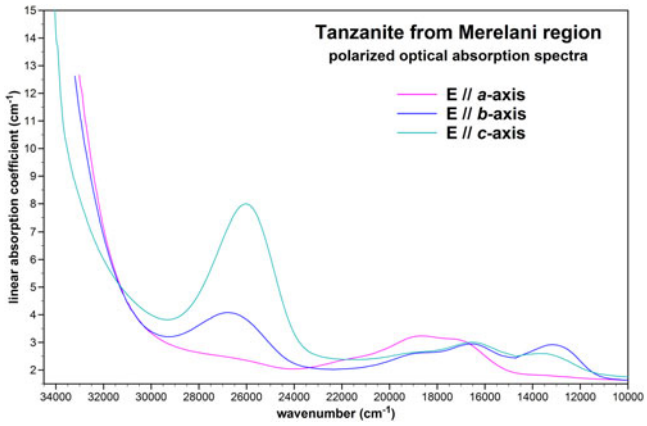

Fig. 3. Polarised optical absorption spectra of tanzanite from the Merelani area, Tanzania.

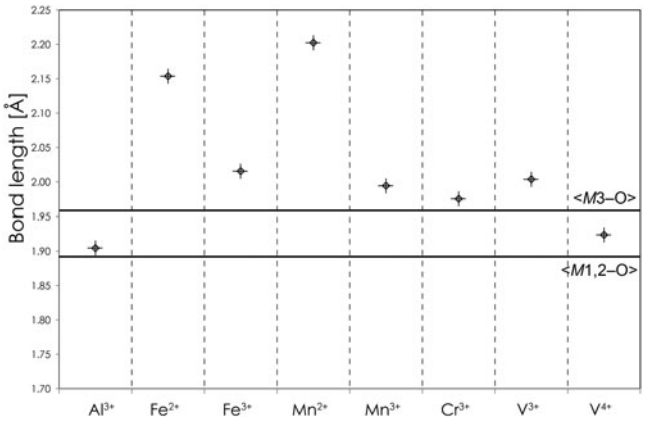

Fig. 4. Calculated bond lengths for selected cations (symbols) compared to empirical average bond lengths for the octahedral sites in zoisite (full horizontal lines).

"the entire *d-d* spectrum of Tanzanian zoisite is in the range ~13000 to 27000 cm^{-1}", and consequently assigned the band systems centred around 13500, 18000 and 27000 cm^{-1} to electronic transitions from the $^3T_1(F)$ ground state of V^{3+} to the excited $^3T_2(F)$, $^3T_1(P)$ and $^3A_2(F)$ levels, respectively. Whereas Faye and Nickel (1971) concluded that V^{3+} only occupies the *M*3 site and hence derived Dq ≈ 1400 cm^{-1} and Racah B <630 cm^{-1}, Tsang and Ghose (1971a) proposed that V^{3+} occupies both Al-sites randomly, resulting in Dq values of 1850 cm^{-1} at the *M*1,2 site and 1400 cm^{-1} at *M*3 (Racah B values were not determined). As part of a comprehensive review on the spectroscopy of epidote-group minerals, Liebscher (2004) gives a detailed summary of the previous studies on the optical absorption spectra of tanzanites.

However, a detailed inspection of the present optical absorption (Fig. 3) combined with crystal chemical arguments and considerations reveals that both the above-mentioned previous interpretations have to be dismissed, at least in part, for the following reasons: (1a) the intense absorption band around 26500 cm^{-1} (Fig. 3), previously assigned as $^3A_2(F)$, definitely shows a minor but unambiguous splitting with maxima around ~26100 (E ∥ *c*) and 26700 cm^{-1} (E ∥ *b*) – this means that it may not be assigned to a non-degenerate A-state which does not split, whatever the local symmetry may be (spin-orbit splitting can also be ignored in case of V^{3+}); (1b) assuming a distribution of V^{3+} on both Al-sites with clearly different Dq-values (as Tsang and Ghose 1971a did) would result in a much larger difference of the two respective $^3A_2(F)$ levels than the mere ~600 cm^{-1} found in the present study; (1c) the $^3T_1(F) \rightarrow {}^3A_2(F)$ transition in d^2 systems corresponds to a forbidden 'two-electron jump' in the classical CF view and is hence expected to be much weaker than the other spin-allowed transitions; in contrast, the band around 26500 cm^{-1} is comparatively intense, especially in polarisation ∥ c, where it is by far the most intense band (Fig. 3).

(2a) Assigning the band around 13500 cm^{-1} to the first spin-allowed band $^3T_1(F) \rightarrow {}^3T_2(F)$ of V^{3+} at the *M*3 site (Faye and Nickel, 1971; Tsang and Ghose, 1971a) leads to an extremely low Dq value of 1350 cm^{-1}, compared to usual values for V^{3+} in oxygen-based compounds (as compiled, e.g. by Wildner *et al.*, 2004) ranging between Dq ≈ 1700–1850 cm^{-1}; (2b) on the contrary, considering the fact that both MO_6 polyhedra in tanzanite have average bond lengths (Table 5) well below the typical octahedral V^{3+}–O distance of 2.01 Å (Schindler *et al.*, 2000), typical or even elevated Dq values are to be expected rather than low ones.

Though the splitting of the band at ~26500 cm^{-1} (points 1a,b,c argued above) has not been observed before, the latter two critical points (2a,b) have already been raised by Schmetzer and Bank (1978) who propose that the band around 13500 cm^{-1} (with partial contribution at ~16000 cm^{-1}) may instead be attributed to V^{4+}. From these revised assignments of the earlier spectra (Faye and Nickel, 1971; Tsang and Ghose, 1971a), Schmetzer (1982) derived Dq = 1917 cm^{-1} and Racah B = 633 cm^{-1} for V^{3+} in tanzanite.

For the present study, we adopt the main features of the interpretation of Schmetzer (1982) and perform semi-empirical CF calculations based on our polarised tanzanite absorption spectra (Fig. 3). The observed transition energies and the energy levels calculated for V^{3+} as well as V^{4+} at both available *M*-sites are summarised in Table 10, together with respective level assignments (for cubic symmetry) and resulting SPM-CF parameters, rotational invariants, Dq_{cub} and (where applicable) Racah B parameters; due to the absence of noticeable spin-forbidden transitions in the tanzanite spectra, Racah C could not be determined.

As Table 10 shows, the SPM-CF calculations for V^{3+} yield good agreements of calculated and observed transition energies for both *M* sites, but especially so for V^{3+} at the *M*1,2 site, thus

Table 9. Calculated ideal bond lengths (in Å) for selected cations in vi, vii and ix coordination, empirical average bond length and their difference (diff.) for each octahedral site in zoisite.

Bond	Bond length	Diff. <*M*1,2–O>	Diff. <*M*3–O>
$^{VI}Al^{3+}$–O	1.9043	0.0130	−0.0536
$^{VI}Fe^{3+}$–O	2.0155	0.1242	0.0576
$^{VI}Mn^{3+}$–O	1.9942	0.1029	0.0362
$^{VI}Cr^{3+}$–O	1.9752	0.0839	0.0173
$^{VI}V^{3+}$–O	2.0036	0.1123	0.0456
$^{VI}V^{2+}$–O	2.1102	0.2189	0.1522
$^{VI}Fe^{2+}$–O	2.1536	0.2623	0.1956
$^{VI}Mn^{2+}$–O	2.2023	0.3110	0.2443
$^{VI}V^{4+}$–O	1.9236	0.0323	−0.0344
<*M*1,2–O>	1.8913		
<*M*3–O>	1.9580		
Bond	**Bond length**	**Diff. <Ca–O>**	**Diff. <Ca–O>**
$^{VII}V^{2+}$–O	2.1102	−0.3965	−0.5205
$^{IX}V^{2+}$–O	2.1102	−0.3035	−0.4275
<Ca1–O>	2.5600		
<Ca2–O>	2.6840		

https://doi.org/10.1180/mgm.2023.48 Published online by Cambridge University Press

Table 10. Observed and calculated transition energies, level assignments for cubic symmetry (with parental terms in parentheses), and obtained crystal field and Racah B parameters for V^{3+} and V^{4+} at both *M* sites in tanzanite.

	Energies (cm^{-1})					Assignments	
Parameter	Observed	Calculated V^{3+} at *M*1,2	Calculated V^{3+} at *M*3	Calculated V^{4+} at *M*1,2	Calculated V^{4+} at *M*3	V^{3+} (cubic)	V^{4+} (cubic)
		0	0	0	0	$^3T_1(F)$	$^2T_2(D)$
		1293	3052	1121	145		
		1658	3239	1741	2677		
	13160			13166	13056		$^2E(D)$
	~15500			15493	15565		
	16350	16702	15149			$^3T_2(F)$	
	16700	16859	15309				
	18800	18338	20779				
	26120	26221	26071			$^3T_1(P)$	
	26650	26346	26231				
		26591	26677				
	34000 ?	35059	33635			$^3A_2(F)$	
R_0 (Å)		2.01	2.01	1.98	1.98		
$\bar{B}_4$ (cm^{-1})		7820	8320	6260	7300		
$\bar{B}_2$ (cm^{-1})		0	0	11600	0		
t_4 / t_2 (fixed)		5 / 3	5 / 3	5 / 3	5 / 3		
s_4 (cm^{-1})		16275	15324	12084	12471		
s_2 (cm^{-1})		0	0	2689	0		
Racah B (cm^{-1})		695	690	–	–		
β (B_0 = 886 cm^{-1})		0.78	0.78	–	–		
Dq_{cub} (from s_4) (cm^{-1})		1776	1672	1318	1362		

hinting to a preference of the latter site. The resulting parameters, Dq_{cub} = 1776 cm^{-1} and Racah B = 695 cm^{-1} comply well with expectations for V^{3+} in oxygen-based structures. However, in calculations for both *M* sites the second-rank parameter $\bar{B}_2$ was refined to $\bar{B}_2$ = 0 cm^{-1}, in gross contradiction to expectations. Generally, $\bar{B}_2 >> \bar{B}_2$ is expected from theory (Newman and Ng, 1989), however in case of $3d^N$ transition ions this sequence is most often not observed, and sometimes $\bar{B}_2 < \bar{B}_4$ is found (Andrut *et al.*, 2004; Wildner *et al.*, 2013). The uncommon values of $\bar{B}_2 = 0$ might also be biased to some extent by the fixation of the power-law exponents t_k to reduce the number of refined parameters, however additional calculations reveal that in the tanzanite spectra the main factor governing $\bar{B}_2$ is the small splitting of the $^3T_1(P)$ level at ~26500 cm^{-1}. In spite of the good agreement of observed and calculated energy levels, a meaningful interpretation of the observed polarisation behaviour in terms of symmetry selection rules is not feasible in view of the low symmetries as well as the irregular distortions of both *M* sites, especially regarding the *M*1,2-site (point symmetry 1) preferred by V^{3+}.

Concerning the results for V^{4+}, the limited number of bands attributable to this d^1-configurated cation and the partial overlapping with the lowest-energy V^{3+}-absorptions do not allow assignation to its preferred *M* site or to extract any further details; the averaged Dq_{cub} value from both sites is 1340 cm^{-1} (Table 10). Similarly, a reliable assessment of the V^{3+}:V^{4+} ratio in the tanzanite sample investigated from the absorption spectra is not possible; therefore, the high intensity of the $^3T_1(P)$ absorption of V^{3+} at ~26500 cm^{-1}, compared to the lowest energy band at ~13100 cm^{-1}, exclusively caused by V^{4+}, indicates that V^{3+} dominates over V^{4+}. Finally, as to the origin of the very weak band found around ~21500 cm^{-1} (in E ∥ *a*), we propose that it represents the remains of a respective intense absorption band typically occurring in untreated tanzanite samples, and tentatively assign it to residual traces of Ti^{3+}, not completely oxidised to Ti^{4+} during heat-treatment.

Bond-Valence Model calculations

The Bond-Valence Model calculation based on the sample structure studied revealed discrepancies between the bond-valence sum and the ideal charge of the site. Bond-valence sum (BVS) calculations at mixed occupancy sites show apparent violations of the Valence Sum Rule (Bosi, 2014). Deviations of the weighted BVS from the weighted sum of formal cation charges results from the difference between the atomic valences and bond-valance parameters (both R_0 and b) of involved cations at the same crystallographic site. The apparent failure of the Valence Sum Rule is expected even for regular and unstrained polyhedra and should be corrected for accurate bond-strain analyses in crystal structures (Bosi, 2014). Such BVS distribution asymmetry between Si1 and Si3, and among Al sites was observed in zoisite (Liebscher *et al.*, 2002) and is analogous to that observed in allanite-group minerals (e.g. Škoda *et al.*, 2012). This results from different local arrangements of individual crystallographic sites.

There are two separate octahedral sites in the zoisite structure – the *M*1,2 site forming the chains parallel to *b* and *M*3 attached to the chain of $M1,2O_6$ octahedra. They differ in the size, bond lengths, bond angles (Fig. 5) and also bond-length and bond-angle distortions (Tables 7, 8). Use of angle variance (σ^2_{oct}) and quadratic elongation (Δ_{oct}) as a measure of distortion was first proposed by (Robinson *et al.*, 1971). The distortion indices (DI), originally defined by Baur (1974) for tetrahedra, were adapted for octahedra by (Wildner, 1992).

The bond-length and bond-angle distortions of the zoisite investigated can be compared with published structures. To avoid any influence from other cations, pure synthetic zoisite was selected (Liebscher *et al.*, 2002). The second structure for comparison is natural zoisite from Merelani with a similar composition to the sample studied but supposedly without heat treatment (Alvaro *et al.*, 2012). In the $M1,2O_6$ octahedron, the value of Δ_{oct} in the sample studied is between the two reference samples. The value of DI(*M*–O) for the sample studied is similar to

https://doi.org/10.1180/mgm.2023.48 Published online by Cambridge University Press

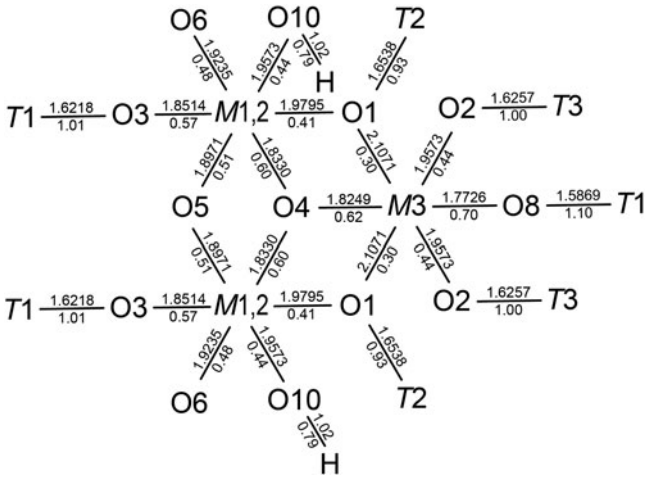

Fig. 5. Bond-topological graphs for *M*1,2 and *M*3 sites and their first and second coordination sphere. The number above the line is the bond length, the number below the line is the bond valence in the studied zoisite.

Table 11. Calculation of individual bond valences (in vu) and lengths (in Å) in both zoisite octahedra occupied by Al^{3+}, V^{3+} and V^{4+}. The Al^{3+}–O bond lengths are empirical from the single-crystal structure refinement, individual V^{3+}–O and V^{4+}–O bond lengths are in the same proportions as Al^{3+}–O.

Cation	Al^{3+}		V^{3+}		V^{4+}	
Bond	Length	Valence	Length	Valence	Length	Valence
*M*1,2–O4	1.8330	0.60	1.9289	0.60	1.8519	0.81
*M*1,2–O-H10	1.9292	0.46	2.0407	0.46	1.9592	0.61
*M*1,2–O3	1.8514	0.57	1.9483	0.57	1.8705	0.77
*M*1,2–O5	1.8971	0.51	1.9964	0.51	1.9167	0.68
*M*1,2–O6	1.9235	0.48	2.0415	0.48	1.9433	0.63
*M*1,2–O1	1.9795	0.41	2.0831	0.41	1.9999	0.54
Average/Sum	1.8871	3.03	2.0036	3.03	1.9236	4.04
Range		0.19		0.19		0.27
*M*3–O8	1.7726	0.70	1.8172	0.79	1.7447	1.09
*M*3–O4	1.8249	0.61	1.8708	0.69	1.7961	0.95
*M*3–O2	1.9573	0.44	2.0066	0.50	1.9265	0.66
*M*3–O2	1.9573	0.44	2.0066	0.50	1.9265	0.66
*M*3–O1	2.1071	0.30	2.1601	0.34	2.0739	0.44
*M*3–O1	2.1071	0.30	2.1601	0.34	2.0739	0.44
Average/Sum	1.9544	2.78	2.0036	3.15	1.9236	4.24
Range		0.40		0.44		0.65

synthetic zoisite (Liebscher *et al.*, 2002) and larger than that of untreated zoisite from Merelani (Alvaro *et al.*, 2012). However, both values of angular distortion, DI(O–*M*–O) and σ^2_{oct}, of the sample studied are the largest in the compared set, whereas the smallest value was found in synthetic zoisite (Liebscher *et al.*, 2002). The situation is different at the *M*3 site. The sample studied has the smallest bond-length distortion, both in terms of Δ_{oct} and DI(*M*–O). The angular distortion of the sample studied is in-between the reference samples, slightly higher than in untreated V-bearing zoisite and smaller than in synthetic zoisite.

On the basis of the geometry of both sites and bond-length calculations, it is possible to divide octahedral cations according to their site preference. It is almost certain that divalent cations including Fe^{2+} and Mn^{2+}, if present, prefer the larger and more distorted *M*3 site. The ideal bond lengths of trivalent cations are closer to the average bond lengths (Fig. 4, Table 9). They differ by 0.084–0.124 Å from <*M*1,2–O> and 0.017–0.058 Å from <*M*3–O> bond lengths. Therefore, it can be assumed that they would prefer the larger octahedral site, but this is not definite. Only V^{4+} has the calculated bond length in the interval between <*M*1,2–O> and <*M*3–O>. Therefore, it is possible that it can occupy both sites. There are no bond-length constraints for that.

As indicated by the bond-length distortion values, the $M3O_6$ octahedron is more distorted, the shortest bond is 1.77 Å, the longest pair exceeds 2.10 Å. The difference in metrics of the $M1,2O_6$ octahedron is smaller, 1.83 *vs.* 1.98 Å (Table 7). Consequently, the differences in bond valences are larger in the $M3O_6$ octahedron (0.70 *vs.* 0.30 vu) than in $M1,2O_6$ (0.41 *vs.* 0.60 vu). Moreover, the *M*1,2 site is slightly overbonded with BVS of 3.03 vu and *M*3 is slightly underbonded (BVS = 2.78 vu). This increases the strength of the $M1,2O_6$ octahedral chains.

If we assume that in the original tanzanite sample, V was trivalent, it should prefer the *M*3 site based strictly on the calculated average bond lengths (Table 9). However, as both octahedra in zoisite are significantly distorted, it is appropriate to calculate bond valences according to the actual octahedral metrics. Original proportions of individual bond lengths in Al^{3+}-bearing octahedra can be used for the calculation of theoretical bond lengths and valences in V^{3+}- and V^{4+}-bearing octahedra (Table 11).

If a similar geometry of both octahedra after the substitution is assumed, we can calculate bond valences for each bond in both octahedra. Trivalent V at *M*1,2 retains its BVS compared to Al^{3+}, if the calculated ideal bond valence is used for the BVS. In contrast, V increases the BVS at the $M3O_6$ octahedron. With the same BVS, the longer V^{3+}–O would induce extension of *M*1,2–O4 and *M*1,2–O6 bonds shared by two neighbouring edge-sharing $M1,2O_6$ octahedra and that would require bond-angle distortion of V^{3+}-bearing or neighbouring octahedra. Considering bond lengths, the *M*3 site is a more natural choice for V^{3+}, because the larger volume and smaller number of shared edges with other octahedra (*M*1,2 – three shared edges, *M*3 – two shared edges) allows greater variability in accommodation of larger cations.

However, if the Bond-Valence Model is considered, a different view can be established. Crystal structures prefer the smallest possible distortions resulting in the smallest energetical requirements for the structural stability. Therefore, the distribution of bond valences for each bond of each ion should be as even as possible. The substitution of ions with the same charge should also not produce too large a difference in the BVS for the specific site. Consequently, if we consider the bond-valence distribution for each bond, V^{3+} at *M*1,2 has bond valences in the range 0.41–0.60 vu (difference of 0.19 vu), which is very similar to Al at this site. However, V^{3+} at the *M*3 site has a significantly larger variation of bond valences (0.34–0.78 vu, i.e. 0.44 vu difference), which is larger than Al (0.40 vu difference) at the *M*3 site. Moreover, the BVS of V^{3+} at *M*3 is significantly larger (3.15 vu) than $^{M3}Al^{3+}$ (2.78 vu). This may indicate the bond-valence distribution requirements result in the preference of the *M*1,2 site for V^{3+}.

A similar consideration can be done with V^{4+}. Logically, the BVS should be ~4, which is the nominal charge of V^{4+}. In both octahedra, the BVS is >4 vu, if the calculated ideal bond valence is used as the BVS. However, the higher BVS value is observed at the *M*3 site of 4.24 vu, which is quite significantly overbonded. Moreover, the *M*3–O8 bond with V^{4+} in *M*3 has more than 1 vu (1.08 vu). As already mentioned, the *M*3–O8 bond is constrained by the Si–O8 bond in the neighbouring tetrahedron. The Si–O8 bond in the zoisite studied is 1.5870 Å with a bond

https://doi.org/10.1180/mgm.2023.48 Published online by Cambridge University Press

valence of 1.08 vu. If its valence was 0.92 vu, which is the subtracted difference of 2 − 1.08 vu, the resulting bond length would have to be >1.65 Å. To obtain such a structural change in the tetrahedron seems unlikely. Moreover, there was no significant shortening of the *M*3–O8 bond observed in the sample studied, it is very similar to untreated zoisite from Merelani. Consequently, V^{4+} at *M*3 site would increase the $M3O_6$ distortion and result in lower structural stability. In contrast, the presence of V^{4+} at the *M*1,2 site does not require significant changes in the octahedral geometry except slight isotropic expansion and seems to be more stable in terms of individual bond valences. This is in accordance with the observed structural data. The studied zoisite has the lowest $M3O_6$ bond-length distortion among compared zoisites and its $M1,2O_6$ bond-length distortion is within the range of the two reference structures (Tables 7 and 8).

The preference of V^{4+} at the *M*1,2 site is supported by the bond-valence distribution; the range of the individual valences is 0.34–0.78 vu (difference of 0.44 vu), which is significantly smaller than 0.44–1.09 vu, i.e. 0.65 vu difference at the *M*3 site. This is similar to V^{3+} and also suggests that V^{4+} at the *M*1,2 site would be more stable from the electrostatic perspective.

The possible presence of V at *M*1,2 also makes sense, if charge-balancing of V^{4+} for Al^{3+} substitution is considered. The cation at *M*1,2 is coordinated by the O10 anion, to which H10 is usually bonded. Therefore, excess in charge due to a four-valent cation can be easily charge-balanced by the deprotonation of O10. This would also influence the bond lengths, mostly *M*1,2–O10 which shortens due to the increase in bond valence after the release of H. In fact, the sample studied has the shortest *M*1,2–O10 bond. This deprotonation should also increase the angular distortion of this octahedron, which was actually observed in the sample studied.

Conclusion

The position of V in the structure of studied heat-treated zoisite var. tanzanite was not possible to determine from the structural refinement. Therefore, advanced theoretical interpretations of structural and optical absorption spectroscopic data were applied. Crystal field Superposition Model calculations from the optical spectra indicated that V^{3+} prefers occupying the *M*1,2 site, however determination of the V^{4+} preference from the present data was not possible. Bond-Valence Model calculations revealed no unambiguous preference for V^{3+}, although the simple bond-length calculation suggests the *M*3-site preference, however it is quite straightforward that the *M*1,2 site is more suitable for V^{4+}. However, if the possible octahedral distortion is considered, the $M1,2O_6$ octahedron is subject to a smaller distortion if occupied by V^{3+} than the $M3O_6$ octahedron. Consequently, considering results of the crystal field Superposition Model and Bond-Valence Model calculations, we propose that both V^{3+} and V^{4+} prefer the *M*1,2 site.

Acknowledgements. The authors thank Andreas Wagner (Vienna) for the careful preparation of the tanzanite crystal slabs for the polarised optical absorption measurements. This work was supported by the Slovak Research and Development Agency under contract No. APVV-18-0065, and VEGA Agency VEGA-1/0137/20 grant. Finally, we thank reviewers and editors for their constructive suggestions for improving the quality of our work.

Supplementary material. The supplementary material for this article can be found at https://doi.org/10.1180/mgm.2023.48.

Competing interests. The authors declare none.

References

Alvaro M., Angel R.J. and Cámara F. (2012) High-pressure behavior of zoisite. *American Mineralogist*, **97**, 1165–1176.

Andreozzi G.B., Lucchesi S. and Graziani G. (2000) Structural study of magnesioaxinite and its crystal-chemical relations with axinite-group minerals. *European Journal of Mineralogy*, **12**, 1185–1194.

Andrut M., Wildner M. and Rudowicz C.Z. (2004) Optical absorption spectroscopy in geosciences: Part II: Quantitative aspects of crystal fields. *Spectroscopic Methods in Mineralogy*, 145–188.

Appel P., Möller A. and Schenk V. (1998) High-pressure granulite facies metamorphism in the Pan-African belt of eastern Tanzania: P-T-t evidence against granulite formation by continent collision. *Journal of Metamorphic Geology*, **16**, 491–509.

Armbruster T., Bonazzi P., Akasaka M., Bermanec V., Chopin C., Gieré R., Heuss-Assbichler S., Liebscher A., Menchetti S., Pan Y. and Pasero M. (2006) Recommended nomenclature of epidote-group minerals. *European Journal of Mineralogy*, **18**, 551–567.

Azavant P. and Lichanot A. (1993) X-ray scattering factors of oxygen and sulfur ions: an abinitio Hartree–Fock calculation. *Acta Crystallographica*, **A49**, 91–97.

Bačík P. and Fridrichová J. (2019) The site occupancy assessment in beryl based on bond-length constraints. *Minerals*, **9**, 641.

Baur W.H. (1974) The geometry of polyhedral distortions. Predictive relationships for the phosphate group. *Acta Crystallographica*, **B30**, 1195–1215.

Bocchio R., Adamo I., Bordoni V., Caucia F. and Diella V. (2012) Gem-quality zoisite from Merelani (Northeastern Tanzania): Review and new data. *Periodico di Mineralogia*, **81**, 379–391.

Bosi F. (2014) Bond valence at mixed occupancy sites. I. Regular polyhedra. *Acta Crystallographica*, **B70**, 864–870.

Brown I.D. (2006) *The Chemical Bond in Inorganic Chemistry*. Oxford University Press, Oxford, UK, 288 pp.

Chang Y.M., Rudowicz C. and Yeung Y.Y. (1994) Crystal field analysis of the $3d^N$ ions at low symmetry sites including the '"imaginary"' terms. *Computers in Physics*, **8**, 583.

Deer W.A., Howie R.A. and Zussman M.A. (1986) *Rock-Forming Minerals, Vol.1b, Disilicates and Ringsilicates*. Longman, UK, 629 pp.

Dirlam D.M., Misiorowski E.B., Tozer R., Stark K.B. and Bassett A.M. (1992) Gem wealth of Tanzania. *Gems & Gemology*, **28**, 80–102.

Dörsam G., Liebscher A., Wunder B., Franz G. and Gottschalk M. (2007) Crystal chemistry of synthetic $Ca_2Al_3Si_3O_{12}OH$–$Sr_2Al_3Si_3O_{12}OH$ solid-solution series of zoisite and clinozoisite. *American Mineralogist*, **92**, 1133–1147.

Faye G.H. and Nickel E.H. (1971) On the pleochroism of vanadium-bearing zoisite from Tanzania. *The Canadian Mineralogist*, **10**, 812–821.

Feneyrol J., Giuliani G., Ohnenstetter D., Fallick A.E., Martelat J.E., Monié P., Dubessy J., Rollion-Bard C., Le Goff E., Malisa E., Rakotondrazafy A.F.M., Pardieu V., Kahn T., Ichang'i D., Venance E., Voarintsoa N.R., Ranatsenho M.M., Simonet C., Omito E., Nyamai C. and Saul M. (2013) New aspects and perspectives on tsavorite deposits. *Ore Geology Reviews*, **53**, 1–25.

Franz G. and Liebscher A. (2004) Physical and chemical properties of the epidote minerals: An introduction. Pp. 1–81 in: *Epidotes* (Axel Liebscher and Gerhard Franz, editors). Reviews in Mineralogy and Geochemistry, **56**. Mineralogical Society of America and the Geochemical Society, Chantilly, Virginia, USA.

Franz G. and Smelik E.A. (1995) Zoisite-clinozoisite bearing pegmatites and their importance for decompressional melting in eclogites. *European Journal of Mineralogy*, **7**, 1421–1436.

Gagné O.C. and Hawthorne F.C. (2015) Comprehensive derivation of bond-valence parameters for ion pairs involving oxygen. *Acta Crystallographica*, **B71**, 562–578.

Gaines R.V., Skinner H.C.W., Foord E.E., Mason B. and Rosenzweig A. (1998) *Dana's New Mineralogy*. Wiley/VCH, New York, 2693 pp.

Ghose S. and Tsang T. (1971) Ordering of V^{2+}, Mn^{2+}, and Fe^{3+} ions in zoisite, $Ca_2Al_3Si_3\ O_{12}(OH)$. *Science*, **171**, 374–376.

Harris C., Hlongwane W., Gule N. and Scheepers R. (2014) Origin of tanzanite and associated gemstone mineralization at Merelani, Tanzania. *South African Journal of Geology*, **117**, 15–30.

Hauzenberger C.A., Bauernhofer A.H., Hoinkes G., Wallbrecher E. and Mathu E.M. (2004) Pan-African high pressure granulites from SE-Kenya: Petrological and geothermobarometric evidence for a polycyclic evolution in the Mozambique belt. *Journal of African Earth Sciences*, **40**, 245–268.

Hauzenberger C.A., Sommer H., Fritz H., Bauerhofer A., Kröner A., Hoinkes G., Wallbrecher E. and Thöni M. (2007) SHRIMP U-Pb zircon and Sm-Nd garnet ages from the granulite-facies basement of SE Kenya: Evidence for Neoproterozoic polycyclic assembly of the Mozambique Belt. *Journal of the Geological Society*, **164**, 189–201.

Jobbins E. A Tresham A E. and Young B. R. (1975) Magnesioaxinite, a new mineral found as a blue gemstone from Tanzania. *Journal of Gemmology*, **14**, 368–375.

Leavitt R.P. (1982) On the role of certain rotational invariants in crystal-field theory. *The Journal of Chemical Physics*, **77**, 1661–1663.

Le Goff E., Deschamps Y. and Guerrot C. (2010) Tectonic implications of new single zircon Pb-Pb evaporation data in the Lossogonoi and Longido ruby-districts, Mozambican metamorphic Belt of north-eastern Tanzania. *Comptes Rendus – Geoscience*, **342**, 36–45.

Liebscher A. (2004) Spectroscopy of epidote minerals. Pp. 125–170 in: *Epidotes* (Axel Liebscher and Gerhard Franz, editors). Reviews in Mineralogy and Geochemistry, **56**. Mineralogical Society of America and the Geochemical Society, Chantilly, Virginia, USA.

Liebscher A., Gottschalk M. and Franz G. (2002) The substitution Fe^{3+}-Al and the isosymmetric displacive phase transition in synthetic zoisite: A powder X-ray and infrared spectroscopy study. *American Mineralogist*, **87**, 909–921.

Malisa E.P. (1998) Application of graphite as a geothermometer in hydrothermally altered metamorphic rocks of the Merelani-Lelatema area, Mozambique Belt, northeastern Tanzania. *Journal of African Earth Sciences*, **26**, 313–316.

Malisa E.P.J. (2004) Trace elements characterization of the hydrothermally deposited tanzanite and green grossular in the Merelani – Lelatema shear zone, northeastern Tanzania. *Tanzania Journal of Science*, **29**, 45–60.

Muhongo S. and Lenoir J.L. (1994) Pan-African granulite-facies metamorphism in the Mozambique Belt of Tanzania: U-Pb zircon geochronology. *Journal of the Geological Society*, **151**, 343–347.

Muhongo S., Tuisku P. and Mtoni Y. (1999) Pan-African pressure-temperature evolution of the Merelani area in the Mozambique Belt in northeast Tanzania. *Journal of African Earth Sciences*, **29**, 353–365.

Newman D.J. (1971) Theory of lanthanide crystal fields. *Advances in Physics*, **20**, 197–256.

Newman D.J. and Ng B. (1989) The superposition model of crystal fields. *Reports on Progress in Physics*, **52**, 699.

Newman D. and Ng B. (2000) *Crystal Field Handbook*. Cambridge University Press, Cambridge, UK, 304 pp.

Pluthametwisute T., Wanthanachaisaeng B., Saiyasombat C. and Sutthirat C. (2020) Cause of Color Modification in Tanzanite after Heat Treatment. *Molecules*, **25**, 3743.

Robinson K., Gibbs G. V. and Ribbe P.H. (1971) Quadratic elongation: A quantitative measure of distortion in coordination polyhedra. *Science*, **172**, 567–570.

Rudowicz C., Yeung Y.Y., Du M.L. and Chang Y.M. (1992) *Manual for the crystal [ligand] field computer package with appendix: Tables of values of the parameters B, C, and ξ for $3d^4$ and $3d^6$ free ions and ions in crystals*. Research Report, Department of Applied Science, City Polytechnic of Hong Kong, Hong Kong, 45 pp.

Rudowicz C., Gnutek P. and Açikgöz M. (2019) Superposition model in electron magnetic resonance spectroscopy–a primer for experimentalists with illustrative applications and literature database. *Applied Spectroscopy Reviews*, **54**, 673–718.

Schindler M., Hawthorne F.C. and Baur W.H. (2000) Crystal chemical aspects of vanadium: Polyhedral geometries, characteristic bond valences, and polymerization of (VO_n) polyhedra. *Chemistry of Materials*, **12**, 1248–1259.

Schmetzer K. (1982) Absorption spectroscopy and colour of V^{3+}-bearing natural oxides and silicates – a contribution to the crystal chemistry of vanadium. *Neues Jahrbuch für Mineralogie – Abhandlungen*, **144**, 73–106.

Schmetzer K. and Bank H. (1978) Bluish–green zoisite from Merelani, Tanzania. *Gems & Gemology*, **16**, 121–122.

Shannon R.D. (1976) Revised effective ionic radii and systematic studies of interatomic distances in halides and chalcogenides. *Acta Crystallographica*, **A32**, 751–767.

Sheldrick G.M. (2015) Crystal structure refinement with SHELXL. *Acta Crystallographica*, **C71**, 3–8.

Škoda R., Cempírek J., Filip J., Novák M., Veselovský F. and Čtvrtlík R. (2012) Allanite-(Nd), $CaNdAl_2Fe^{2+}(SiO_4)(Si_2O_7)O(OH)$, a new mineral from Åskagen, Sweden. *American Mineralogist*, **97**, 983–988.

Tsang T. and Ghose S. (1971a) Electron paramagnetic resonance of V^{2+}, Mn^{2+}, Fe^{3+}, and optical spectra of V^{3+} in blue zoisite, $Ca_2Al_3Si_3O_{12}(OH)$. *The Journal of Chemical Physics*, **54**, 856–862.

Tsang T. and Ghose S. (1971b) Ordering of transition metal ions in zoisite. *Eos Transactions American Geophysical Union*, **52**, 380–381.

Wildner M. (1992) On the geometry of $Co(II)O_6$ polyhedra in inorganic compounds. *Zeitschrift für Kristallographie – Crystalline Materials*, **202**, 51–70.

Wildner M., Andrut M. and Rudowicz C.Z. (2004) Optical absorption spectroscopy in geosciences. Part I: Basic concepts of crystal field theory. pp. 93–143 in:*Spectroscopic Methods in Mineralogy* (Anton Beran and Eugen Libowitzk, editors). EMU Notes In Mineralogy, **6**, European Mineralogical Union.

Wildner M., Beran A. and Koller F. (2013) Spectroscopic characterisation and crystal field calculations of varicoloured kyanites from Loliondo, Tanzania. *Mineralogy and Petrology*, **107**, 289–310.

Yang Z.Y., Hao Y., Rudowicz C. and Yeung Y.Y. (2004) Theoretical investigations of the microscopic spin Hamiltonian parameters including the spin-spin and spin-other-orbit interactions for $Ni^{2+}(3d^8)$ ions in trigonal crystal fields. *Journal of Physics Condensed Matter*, **16**, 3481–3494.

Yang S., Ye H., Liu Y., Lu T., Liu F., Gu T. and Gurzhiy V. V. (2021) The different inclusions′ characteristics between natural and heat-treated tanzanite: evidence from Raman spectroscopy. *Crystals*, **11**, 1302.

Zancanella V. (2004) *Tanzanite: una tra le gemme più affascinanti*. Raffaele Zanacanella s.r.l. edition, Cavalese, Italy, 118 pp.

https://doi.org/10.1180/mgm.2023.48 Published online by Cambridge University Press